applied optics

Low-volume, fast response-time hollow silica waveguide gas cells for mid-IR spectroscopy

Daniel Francis,[1] Jane Hodgkinson,[1,*] Beth Livingstone,[2] Paul Black,[2] and Ralph P. Tatam[1]

[1]Engineering Photonics, Cranfield University, Cranfield, Bedfordshire MK43 0AL, UK
[2]Cascade Technologies, Glendevon House, Castle Business Park, Stirling FK9 4TZ, UK
*Corresponding author: j.hodgkinson@cranfield.ac.uk

Received 13 May 2016; revised 20 July 2016; accepted 28 July 2016; posted 28 July 2016 (Doc. ID 265137); published 22 August 2016

Hollow silica waveguides (HSWs) are used to produce long path length, low-volume gas cells, and are demonstrated with quantum cascade laser spectroscopy. Absorption measurements are made using the intrapulse technique, which allows measurements to be made across a single laser pulse. Simultaneous laser light and gas coupling is achieved through the modification of commercially available gas fittings with low dead volume. Three HSW gas cell configurations with different path lengths and internal diameters are analyzed and compared with a 30 m path length astigmatic Herriott cell. Limit of detection measurements are made for the gas cells using methane at a wavelength 7.82 μm. The lowest limit of detection was provided by HSW with a bore diameter of 1000 μm and a path length of 5 m and was measured to be 0.26 ppm, with a noise equivalent absorbance of 4.1×10^{-4}. The long-term stability of the HSW and Herriott cells is compared through analysis of the Allan–Werle variance of data collected over a 24 h period. The response times of the HSW and Herriott cells are measured to be 0.8 s and 36 s, respectively.

OCIS codes: (120.6200) Spectrometers and spectroscopic instrumentation; (300.6340) Spectroscopy, infrared; (060.2390) Fiber optics, infrared.

http://dx.doi.org/10.1364/AO.55.006797

1. INTRODUCTION

Tunable diode laser spectroscopy (TDLS) [1,2] is a sensitive and highly selective technique used for the measurement of molecular concentrations of a range of gas species [3]. It relies on the absorption of light at specific wavelengths determined by the molecular properties of the species of interest. The strongest absorption features of many species lie in the mid-infrared region of the electromagnetic spectrum at about 3–12 μm. Difficulties developing reliable tunable lasers in the mid-IR has meant that laser spectroscopy historically tended to focus on weaker overtone features in the near-IR where lasers and detectors are lower cost and more efficient. The advent [4] and development [5] of the quantum cascade laser (QCL), which offers high-power, tunable, pulsed, or cw radiation at wavelengths ranging from 3.5 to 19 μm, has opened up this region. As a consequence, mid-IR spectroscopy is a rapidly developing area of research. The applications of mid-IR spectroscopy are numerous and feature in areas including environmental monitoring [6], medical diagnostics [7,8], and security [9]. In some applications, such as headspace [10] or breath [11] analysis, only small volumes of the gas of interest are available. Therefore, gas cells with a low volume and a fast response time, which retain the long path length that gives absorption spectroscopy its sensitivity, are highly desirable.

The use of hollow silica waveguides (HSWs) for the construction of low-volume gas cells has become better established over recent years [12] but has yet to fully develop into a mature technology. HSWs were initially developed for guiding high-power infrared light from sources such as CO_2 (10.6 μm) or Er:YAG lasers (2.94 μm) [13]. These waveguides consist of a silica tube with bore diameters ranging from around 250 μm [14] up to about 1000 μm [15]. A wet chemistry technique [16] is used to deposit a layer of silver that is then exposed to a halogen, often iodine, which converts some of the silver to a silver halide. This can improve wall reflectivity at infrared wavelengths by more than an order of magnitude. The thickness of the halide layer determines the spectral characteristics of the waveguide so that they can be designed with a particular application wavelength in mind [17]. Alternating multiple dielectric layers of high and low refractive index has shown the potential to further reduce transmission losses [18]. The thickness of the metal/dielectric coating is usually around 1 μm, with the halide layer ranging from 20% to 80% of this. A schematic showing the construction of a typical HSW, with thickness values taken from the commercially available range from Polymicro Technologies [19], is shown in Fig. 1.

A number of authors have reported the use of hollow waveguide gas cells in spectroscopy using Fourier transform infrared

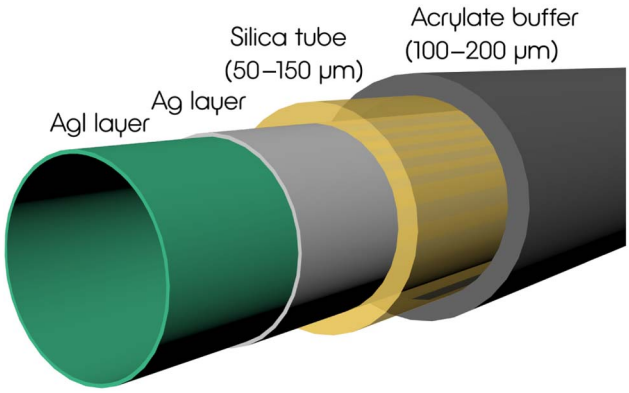

Fig. 1. Schematic showing the construction of a hollow silica waveguide. The values indicate the radial thicknesses of the silica and acrylate of the smallest (300 μm bore diameter) and largest (1000 μm bore diameter) commercially available waveguides from Polymicro Technologies [19].

(FTIR) and TDLS with QCLs. These cells have a very large path length to volume ratio, particularly in comparison to well-known multipass cells such as Herriott or White cells [3], which means that much faster response times and/or lower flow rates can be achieved without significantly compromising the signal-to-noise ratio. Fetzer *et al.* [20] describes spectroscopy of CO_2 and NH_3 using coiled hollow waveguide gas cells with a distributed feedback (DFB) laser operating at around 1.5 μm. A 3 m long, 1000 μm bore diameter waveguide was used that was optimized for Er:YAG delivery (2.94 μm). This was inefficient at the application wavelength, but sufficient transmission was achieved to perform measurements. Charlton *et al.* [21] used a 4 m path length hollow waveguide gas cell and a QCL for spectroscopy of ethyl chloride at 10.3 μm and obtained a limit of detection of 0.5 ppm. Young *et al.* [22] used an external cavity QCL (EC-QCL) with a hollow waveguide gas cell for multi-analyte sensing over the spectral range of 7.71–8.20 μm with detection limits at the parts per billion (ppb) level. Thompson *et al.* [23] used an in-house-developed, 2100 μm bore diameter hollow waveguide with an FTIR for spectroscopy of CO and measured an order of magnitude improvement in response time when compared with a 3 m multipass cell. Chen *et al.* [24] describe a system incorporating a vertical cavity surface emitting laser (VCSEL) (1.68 μm and 2.37 μm) and a hollow waveguide gas cell with a bore diameter of 750 μm. They observed significant speckle noise associated with multimode interference that limited absorption measurements, made with a second harmonic modulation scheme, to 1×10^{-4}. Vibrating the waveguide to reduce speckle noise improved the signal-to-noise ratio by an order of magnitude.

An alternative to HSWs in the development of low-volume gas cells are various types of photonic crystal fiber. Photonic bandgap fibers [25] (PBGFs), which guide light via photonic bandgap effects rather than total internal reflection, are particularly suited to gas sensing due to a hollow air core. Typical PBGFs consist of a central hollow core with diameters typically in the range of 10–40 μm surrounded by a microstructured lattice that provides the photonic crystal properties. PBGF gas cells [26] offer tremendous potential due to their very low attenuation (tens of dB/km), which is substantially better than can be achieved with HSW. They currently have two major limitations. First, the small core (when compared to HSW) means that the response times can be very slow. Parry *et al.* [27] report a fill time of 20 min for a 90 cm PBGF gas cell that incorporated laser-drilled holes in the side wall to aid diffusion. The other issue is their spectral range of operation; PBGFs are generally designed to operate at telecoms wavelengths around 1.5 μm, and fibers working in the mid-IR are currently only in the development stage. Recently, a PBGF gas cell has been used for CO_2 detection at 2 μm [28], and transmission has been demonstrated up to 3.7 μm [29]. In between HSW and PBGF is the photonic bandgap OmniGuide [30]. These consist of alternating cylindrical layers of dielectric materials of different refractive indices around a central hollow core and are based on the omnidirectional mirror [31], which achieved very low loss over a spectral region of 10–15 μm. These have much larger cores than PBGFs and work at longer wavelengths but do not have good attenuation characteristics. Charlton *et al.* [32] describe the use of an OmniGuide gas cell that was 1 m long and had a 700 μm internal diameter. It was used to measure ethyl chloride at 10.3 μm with a limit of detection of 30 ppb.

Another alternative that has recently been reported [33] is the surface-integrated hollow waveguide (iHWG). This consists of a metallic substrate into which a narrow (~2 mm) diameter coiled channel has been machined, which serves as a light pipe. The substrate is sputter-coated with gold to improve its reflectivity and is sealed with a matching substrate into which gas entry and exit ports are introduced. The iHWG has a 22 cm path length in a 75 × 50 × 12 mm footprint and has successfully been used for carbon dioxide isotopologue ratio measurements in exhaled mouse breath [34], where the volume of usable gas is only ~0.6 ml. Gas cells made from the iHWG provide excellent modularity and mechanical stability compared to those made from HSW and present a much smaller footprint than HSW with a similar bore diameter. They were developed as a response to vibration stability issues with gas cells made with HSW. However, available path lengths are shorter than for HSW (22 cm compared to 5 m), and losses per unit length are higher than that achieved with HSW. There are essentially two methods of reducing attenuation within hollow waveguide gas cells: one is to reduce the number of reflections experienced throughout transmission and the other is to reduce the attenuation associated with each reflection. By using a channel with a diameter that is much larger than HSW with a similar footprint, the iHSW addresses this issue with the first method, whereas HSW with its high reflectivity dielectric coating addresses the issue with the second method. Which of the two devices has the highest path-length-to-loss ratio is not yet known. A summary of the different properties of the hollow waveguide gas cells discussed here is given in Table 1.

HSWs offer great potential for low-volume gas cells for use in the mid-IR; however, they can suffer from instability/vibration owing to their multimode nature if coiled [35] or if their bore diameter is more than ~30 times the application wavelength [18]. Here we use HSW gas cells with a high-frequency (50–100 kHz) modulation technique that minimizes these

Table 1. Summary of Hollow-Waveguide-Based Gas Sensors Used in Infrared Spectroscopy

Source	Wavelength	Cell Type	Cell Bore	Cell Length	Species	LoD	Ref
DFB	1.5 μm	HSW	1000 μm	3 m	CO_2, NH_3	3.5×10^{-5} NEA	[20]
QCL	10.3 μm	HSW	700 μm	4 m	C_2H_5Cl	0.5 ppm	[21]
EC-QCL	7.7–8.2 μm	HSW			organics	~ppb	[22]
FTIR		HSW	2,100 μm		CO		[23]
VCSEL	1.68/2.37 μm	HSW	750 μm		CH_4, H_2O	1×10^{-5} NEA	[24]
DFB	1.65 μm	PBGF		90 cm	CH_4		[27]
DFB	2 μm	PBGF	15 μm	5.27 m	CO_2	59 ppm · m	[28]
QCL	10.3 μm	OmniGuide	700 μm	1 m	C_2H_5Cl	30 ppb	[32]
FTIR		iHSW	~2 mm	22 cm	Organics	6–21 ppm	[33]

effects, making the cells more suited to real world environments. The work that we describe in this paper differs from previous work in that it makes use of the intrapulse modulation technique for QCLs [36]. The principle advantage of this method is that it provides a full spectral scan within the submicrosecond timeframe of a single pulse. Thus, changes to the spectral baseline that might be caused by vibration, for example, are reduced since the spectrum is self-referenced on a much shorter timescale than that which typically applies to mechanical vibration. Use of the intrapulse technique then raises the question as to what level of performance is achievable; HSWs suffer from significant transmission losses, and bend losses when coiled, resulting in relatively low throughput compared to other gas cells. At the same time, the use of high-bandwidth detection electronics required for nanosecond intrapulse resolution can compromise the detector gain and therefore noise levels. An aim of this work was to investigate the achievable performance with the intrapulse technique.

One of the key engineering challenges associated with the construction of HSW gas cells is to devise a way of coupling both the light and the gas into the waveguide simultaneously while minimizing the dead volume at the input and output ends, which would otherwise cancel the benefit of the low-volume waveguide. While this problem has been solved in previously presented work, it has not been explicitly described. Fetzer *et al.* [20] used a CO_2 laser to perforate the wall of the waveguide to allow an array of gas entry/exit points and used O-rings and either a lens or a window to provide sealing and also allow light into the waveguide. However, the ends of the system were not explicitly coupled to the gas supply and represent potential dead space in the system. Saito and Kato [37] describe a hollow waveguide gas cell with metal holders at each end, which allow gas in and out. The holders house a calcium fluoride (CaF_2) window to allow light in and out. Charlton *et al.* [21] describe custom-made gas cells with zinc selenide (ZnSe) windows into which each end of the waveguide is sealed. They mention a low dead volume of <5 mm^3; however, there is no discussion of how these gas cells are constructed or how they are fitted to the waveguide. Our method involves the modification of standard elbow union gas fittings, which have the advantage of making the cells compatible with standard gas supply systems while minimizing the dead volume within the cell [38].

In this paper, we present a simple and effective solution based on the modification of commercially available gas fittings. These modified fittings, presented in Section 3, are small and robust and have the additional benefit of being compatible with existing gas pipework. Section 4 describes the limit of detection measurements made with a range of HSW gas cells. Their performance, in terms of stability and response time, is compared with that of an astigmatic Herriott cell in Section 5.

2. INTRAPULSE SPECTROSCOPY

The work presented here employed a Cascade Technologies [39] CT3000 gas analysis platform, which incorporates a QCL that emits pulsed radiation with a center wavelength of 7.82 μm at a control temperature of 25°C. The platform is capable of housing up to three additional lasers, which can be collimated, aligned on a single axis, and run simultaneously for multispecies analysis. For our work, only a single channel at 7.82 was installed. Therefore, we did not test multiwavelength operation. A mercury cadmium telluride [(HgCd)Te] thermoelectrically cooled photodetector with a detectivity of 2.6×10^9 cm Hz$^{1/2}$/W was used in conjunction with the laser system. The spectroscopic principle that the system utilizes is based on that described by Normand *et al.* [36]. The application of a top-hat current pulse to the QCL, with typical durations in the range from 100 to 1000 ns, results in a thermal variation across the laser chip. This causes a gradual reduction in frequency (down-chirp) across the pulse that can be used to scan across an absorption line of the gas species of interest. Spectral absorption occurs according to the Beer–Lambert law, which relates absorption to the concentration of the gas present and the path length through which the light travels as

$$I = I_0 \exp(\alpha l), \tag{1}$$

where I is the transmitted intensity, I_0 is the intensity prior to interaction with the gas, α is the concentration-dependent absorption coefficient (in units cm^{-1}), and l is the optical path length (in units cm). At atmospheric pressure, the spectral absorption profile α follows a pressure-broadened Lorentzian distribution described by [3]

$$\alpha = C_{\text{mol}} \frac{S\gamma}{\pi[\gamma^2 + (\nu - \nu_0)^2]}, \tag{2}$$

where C_{mol} is the molar concentration, S is spectral line intensity (cm/molecule), γ is the half-width at half-maximum (HWHM) of the gas line (cm^{-1}), ν is the optical frequency in wavenumbers (cm^{-1}), and ν_0 is the center frequency of the gas line.

The frequency down-chirp technique is often referred to as the intrapulse technique because the wavelength tuning occurs over the duration of a single pulse and differs from the

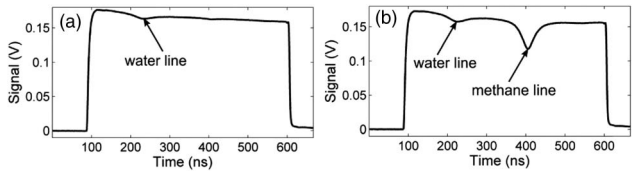

Fig. 2. Intrapulse QCL spectroscopy. Typical traces obtained from the average of 1000 pulses recorded in (a) laboratory air and (b) with the beam passing through 2.5% methane in a 165 mm path length gas cell.

interpulse technique in which the output is wavelength tuned by modulation of the control current [40] in between the emission of short duration (~10 ns) laser pulses. The main advantages of the intrapulse technique are its improved linearity and the provision of a wider spectral window allowing the capture of more spectral information within a single laser pulse [41]. The spectral resolutions of the two techniques are similar; however, the resolution of the intrapulse technique can be improved by slowing the chirp rate, as demonstrated in [41]. The spectral resolution is dependent on the chirp rate and the time–bandwidth product, which for a bandwidth-limited Gaussian is ≈0.44. To achieve time–bandwidth-limited resolution, fast (>100 MHz) detectors are required in order to resolve the temporal variation of the pulse signal. High-speed detection means that single spectra acquisition can be made at rates up to hundreds of kilohertz, which facilitates averaging of thousands of pulses, significantly improving the signal-to-noise ratio. An additional benefit of the high repetition rates is that the recorded spectra are relatively unaffected by most typical lower frequency mechanical vibrations [hertz–kilohertz (Hz–kHz)]. This is a known issue for use of HSW gas cells with lower frequency measurements, e.g., traditional harmonic laser modulation techniques [20] and FTIR [10].

The chirp rate of the laser is 3×10^{-3} cm^{-1}/ns (90 MHz/ns), which means that for a 500 ns pulse at 25°C, the wavelength variation across the pulse is 9.2 nm. The temperature tuning rate is 0.09 $cm^{-1}/°C$, which results in a wavelength range of 27.5 nm for a temperature range of 50°C. The analog-to-digital converter used has 8 bit digital resolution and a 750 MHz data rate, which provides a temporal resolution of 1.33 ns. Figure 2 shows some examples of digitized pulses of 500 ns duration captured at a rate of 50 kHz and recorded with the detector. The traces shown consist of an average of 1000 pulses, which account for the low noise content in the plots. Figure 2(a) was obtained with laser light directly incident on the detector with the QCL's thermoelectric cooler (TEC) set at 15°C. The small absorption feature at ~230 ns is caused by water present in the laboratory air. Figure 2(b) shows a trace obtained with the beam passing first through a 165 mm path length, single-pass gas cell containing 2.5% methane in air. The water line is still present and additionally the weak methane line centered at 7.814 nm (1279.8 cm^{-1}) can be seen at ~400 ns.

3. CONSTRUCTION OF HOLLOW SILICA WAVEGUIDE GAS CELLS

The gas cells considered here were made using HSWs purchased from Polymicro Technologies [19]. Each waveguide has a length of 5 m, which is the maximum available. Two waveguide types were used, with bore diameters of 300 μm and 1000 μm and outer diameters of 600 μm and 1700 μm, respectively. The smaller waveguide is considerably more flexible, with a minimum coil diameter of ~25 mm compared with the minimum coil radius of the larger waveguide of ~150 mm. The smaller waveguide experiences greater attenuation, however, due to a $1/a^3$ dependence on bore diameter a and a $1/R$ dependence on bend radius R [17].

The principle behind the idea is illustrated in Fig. 3 and involves machining the fitting opposite one of the connections so that a window can be adhered. CaF_2 windows were chosen because they exhibit good transmission at 7.82 μm, are nontoxic (unlike ZnSe), and transparent in the visible region of the spectrum (unlike Ge). The corner of the fitting was machined so as to allow attachment of a window. The end of the waveguide was inserted into a section of stainless steel tube of the correct diameter for the gas fitting used and then fitted into the elbow at the opposite end to the window. A second modified fitting constructed identically was connected at the opposite end of the waveguide, allowing for entry and exit ports.

Two gas fitting port designs were implemented, which are illustrated schematically in Fig. 4. Figure 4(a) shows the fitting machined at the Brewster angle ($\theta_B = 53.5°$ at 7.82 μm for CaF_2) and uses 15 mm diameter windows. This serves to reduce the influence of interference fringes caused by reflections within the window, and the machining can be done to a tolerance of ±0.5°. Figure 4(b) shows a 5 mm diameter window recessed into the fitting oriented approximately normal to the optical axis. This design is more compact and easier to handle since there is no window material protruding from the edges of the fitting. Both designs were constructed and tested.

A 5 m gas cell was constructed using the 1000 μm bore diameter HSW with ports made using 1/8 in. (1 in. = 2.54 cm) gas fittings. Each end of the waveguide was inserted into a short stainless steel tube, which has a wall thickness of 0.7 mm and an inner diameter of 1.725 mm. The Swagelok elbow union fitting was then fastened onto the tube, and the opposite end of the tube was sealed with a metal-loaded epoxy (RS Components). A photograph of one of these fittings is shown in Fig. 4(c). Alignment of the light entry point was achieved by clamping the stainless steel tube rather than the fitting itself. This was done using PTFE disks made in-house, which were held using

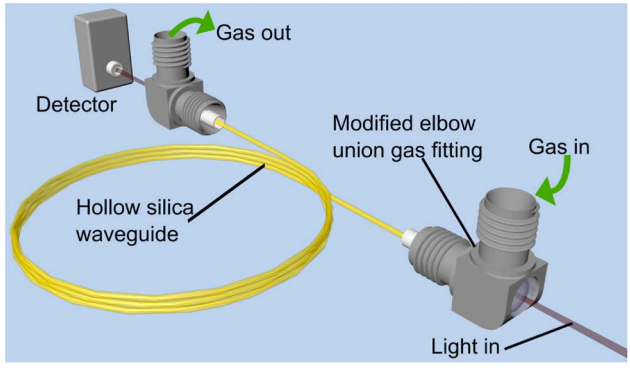

Fig. 3. HSW gas cell constructed using modified gas fittings. The size of the fittings is exaggerated in the image.

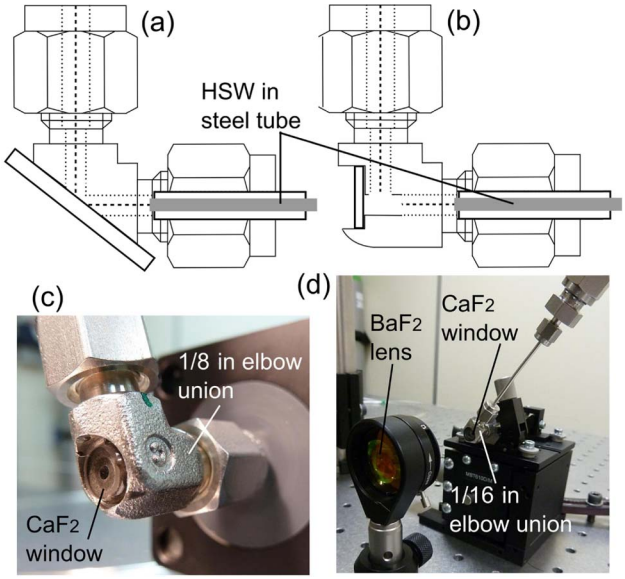

Fig. 4. Designs for modified Swagelok fitting gas and light entry and exit ports. Brewster-angled machining with (a) 15 mm CaF_2 windows and (b) recessed 5 mm windows. The photographs show ports built with recessed 5 mm windows using (c) 1/8 in. fittings with the 1000 μm bore HSW and (d) using 1/16 in. fittings with the 300 μm bore HSW. Drawings shown in (a) and (b) are redrawn and modified versions of images obtained from [42].

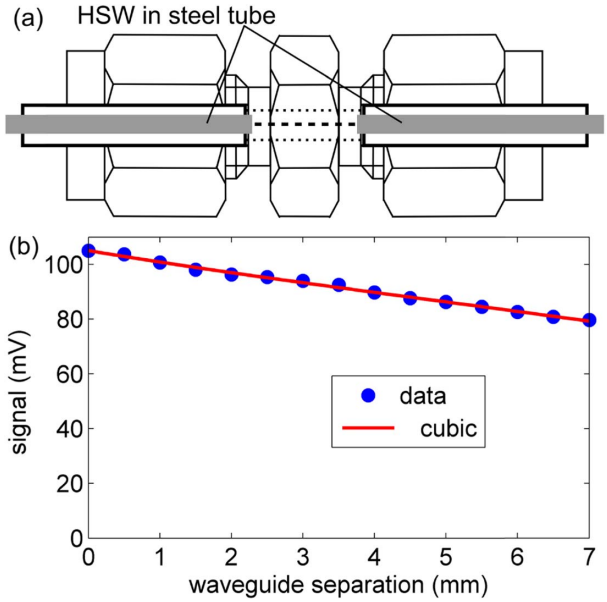

Fig. 5. (a) Design for the use of a straight union gas fitting to connect two sections of HSW to produce a 10 m long gas cell. Redrawn and modified version of the image obtained from [42]. (b) Experimental data showing signal attenuation associated with the gap introduced between two sections of waveguide and a cubic fit.

MicroBench lens holders, as can be seen in Fig. 4(c). Coupling light into the waveguides is best achieved with lenses with relatively low numerical aperture (NA). The coupling lens that was used was a BaF_2 optic with a focal length of 150 mm, which was mounted outside the cell. External mounting is beneficial to alignment and could not be achieved if a high-NA launch was required.

A longer, 10 m path length gas cell was also constructed by connecting two 5 m waveguide sections. The connection was sealed by placing a short length of steel tubing with a gas fitting attached to it at the two waveguide ends that made up the connection. These were held together using a 1/8 in. (3.18 mm) straight union connector, as shown in Fig. 5(a). Alternatively, a T-piece gas fitting could be used to make the connection, which would allow an additional gas inlet/outlet. The gap between the two sections of waveguide introduces additional loss, and this was measured by holding two 5 m waveguide sections in three-axis micropositioners. The signal arriving at a detector placed at the output of the second waveguide section was monitored as the gap between the two sections was increased. The results of these measurements are shown plotted in Fig. 5(b), with measurements made at 0.5 mm increments and fitted with a cubic polynomial. The gap that exists between the waveguide sections held in the union for the 10 m cell is ∼3 mm, so a loss of ∼15% can be attributed to the gap. While significant, this loss is not sufficient enough to prevent the construction of a functional 10 m gas cell. Indeed, the main contribution to the overall loss in the 10 m cell relative to the 5 m cell is the added length of the waveguide itself. The fact that the loss at the gap is not more severe is largely attributable to the low NA of the HSW. The gas cell made using the 300 μm bore diameter HSW was built using 1/16 in. (1.59 mm) elbow unions that were fitted to short sections of stainless steel tubing with a 1/16 in. outer diameter and an inner diameter of 0.040 in. (1 mm). Stainless steel tubing of these dimensions is quite malleable. Therefore, it was quite difficult to produce perfectly straight short sections for the gas cell. This had an impact on alignment of the cell with the input laser light and the positioning of the detector. The tubing sections were, however, small enough to be held in micropositioners (rather than lens holders), which have fine, three-axis adjustments that helped somewhat with alignment [shown in Fig. 4(d)]. A higher NA, 50 mm focal length coupling lens was used to launch light into this smaller waveguide. However, the NA was still sufficiently low to mount it externally to the cell. The coil diameters of the gas cells constructed using the 1000 μm and 300 μm bore diameter HSWs were ∼30 cm and 15 cm, respectively.

4. COMPARISON OF HOLLOW SILICA WAVEGUIDE GAS CELLS

The performance of the three different HSW gas cells was assessed by using methane as a test gas and a network of mass flow controllers (MFCs) (Teledyne Hastings 301) controlled by a Teledyne THPS-400-230 unit. These were used to dilute the methane by factors of up to a thousand and allowed measurements of the limit of detection for each of the cells.

A. Testing Methodology

The system performance was tested by spectroscopic analysis of the methane line pair centered at 7.828 and 7.832 μm (1277.47 cm^{-1} and 1276.84 cm^{-1}). These are the strongest

methane lines within the tuning range of the laser, with line intensities of 3.74×10^{-20} cm/molecule and 3.73×10^{-20} cm/molecule, respectively [43]. For each gas cell configuration, a series of spectroscopic measurements was made with gradually reduced methane concentration achieved by diluting with hydrocarbon-free air with a specified total hydrocarbon concentration of less than 0.1 ppm. Measurements were made at a constant total flow rate of 1000 sccm.

For these measurements, the laser pulse width was set at 800 ns with a TEC temperature of 44°C, which was sufficient to cover both of the methane absorption features within the spectral window of the pulse down-chirp. The pulse repetition frequency was 50 kHz and 1000 pulses were averaged. Averaged sets of 1000 pulses were recorded every 2 s, and at each concentration step, 60 such averaged measurements were taken. The ambient temperature and pressure was monitored throughout, with readings being taken roughly every 30 min. The temperature and pressure over the entire course of the experiments, carried out over several days, varied between 24.5°C and 26.0°C and 994 to 1009 mb, with a maximum fluctuation of ±0.5°C and ±1 mb over a single experiment, each of which took ~2 h. We did not monitor the pressure inside the cell, but did not observe any resistance to gas flow or any change to gas line shapes when the flow was halted, which would have allowed any internal pressure to relax. The sample gas exited the cell at atmospheric pressure. Methane from two cylinders was used, with base concentrations of 1000 ppm (0.1%) and 50 ppm.

B. Data Processing

The noise equivalent absorbance (NEA) ($\Delta I/I$) for each cell using the normal recessed windows was calculated from the acquired pulse data and was found to be 4.1×10^{-4} for the 1000 μm bore diameter, 5 m path length gas cell; 1.8×10^{-3} for the 1000 μm bore diameter, 10 m path length gas cell; and 1.7×10^{-3} for the 300 μm bore diameter, 5 m path length gas cell. The increase in NEA for the 1000 μm bore diameter, 10 m path length gas cell relative to the 5 m path length cell is due to attenuation in the waveguide resulting in approximately an order of magnitude less optical radiation arriving at the detector. Similarly, the NEA of the 300 μm bore diameter gas cell is greater than the 1000 μm bore diameter gas cell again because of optical loss, this time due to bore-diameter-dependent attenuation, which varies as $1/a^3$.

To calculate the normalized absorption, a series of 20 consecutive measurements was taken, corresponding to a period of 40 s. This period was sufficient to ensure that the cell was full and that the concentration had stabilized. The normalized absorption at each wavelength was calculated using

$$A = -\ln\left(\frac{V_{CH_4}}{V_{air}}\right), \tag{3}$$

where V_{CH_4} is the signal voltage for the methane data, and V_{air} is the signal voltage for the zero air data. The normalized absorption calculated for methane concentrations within the range of 1000 to 100 ppm is shown in Fig. 6(a), and the range of 10 to 1 ppm is shown in Fig. 6(b). These measurements were made using methane with an initial concentration of 1000 ppm. The concentration values shown were calculated from the methane and air flow rates emitted by the MFCs and are noninteger due to a difference between the set and actual flow rates. Noise is much more apparent on the absorption profiles in Fig. 7(b), where the methane concentration is below 10 ppm. The absorption features are still clearly visible, however, and only begin to become obscured at around 1–2 ppm.

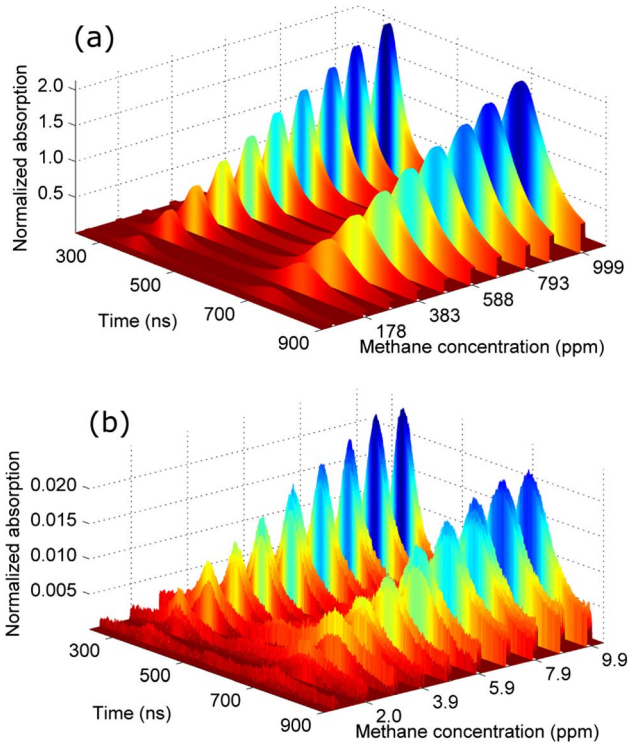

Fig. 6. Normalized absorption profiles calculated from the data shown in Fig. 6 for (a) the high concentration range (~1000 to 100 ppm) and (b) the low concentration range (~10 to 1 ppm).

Since the measurements were carried out at room temperature and pressure, the absorption profiles can be fitted to a Lorentzian function. The close proximity of the two peaks means that one has the potential to influence the other. Therefore, least-squares fits were made to a dual Lorentzian function given by

$$F(x) = \frac{p_1}{\pi}\left[\frac{p_3^2}{(x-p_2)^2+p_3^2}\right] + \frac{p_4}{\pi}\left[\frac{p_6^2}{(x-p_5)^2+p_6^2}\right] + C. \tag{4}$$

Here, p_1 and p_4 correspond to the peak magnitude, p_2 and p_5 correspond to the HWHM, p_3 and p_6 correspond to the

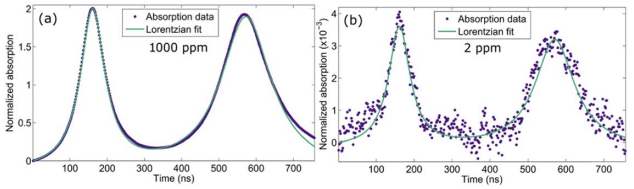

Fig. 7. Normalized absorption data with the corresponding Lorentzian functions fitted to both peaks. The data were obtained in the presence of methane at concentrations of (a) 1000 ppm and (b) 2 ppm.

peak position, and C is a constant. The parameters $p_1 - p_6$ were given starting values and then allowed to vary to best match the measured absorption profiles using the minimum least-squares algorithm in MATLAB. Some examples of normalized absorption profiles and their fits are shown in Fig. 7. Normalized absorption data obtained in the presence of 1000 and 2 ppm methane are shown in Figs. 7(a) and 7(b), respectively, along with the corresponding fits to the function given in Eq. (3). As expected, the data are noisier at 2 ppm relative to 1000 ppm; however, the absorption peaks are still clearly visible and the fit still works well.

Quantitative concentration measurements were obtained from the measured absorptions α using

$$\alpha = C_{\text{mol}}\left(\frac{S_1\gamma_1}{\pi[\gamma_1^2 + (\nu - \nu_{01})^2]} + \frac{S_2\gamma_2}{\pi[\gamma_2^2 + (\nu - \nu_{02})^2]}\right), \quad (5)$$

where the parameters are as defined for Eq. (2) for the absorption lines 1 and 2, respectively. The S, γ, and ν parameters for these specific lines are available in the HITRAN database [42]. Air-broadened half-widths were used here, rather than self-broadened half-widths because the highest methane concentration that was investigated was 0.1%. Therefore, the mixture was mostly air at all concentration levels.

To obtain a measure of the concentration at each step, the Lorentzian fit to the measured absorption coefficient data was integrated over the wavelength range covered by the spectral window provided by the frequency down-chirp. The Lorentzian distribution associated with the parameters obtained from HITRAN was calculated and also integrated over the same wavelength range. The ratio of these two values yields the concentration C_{mol} in terms of molecules per cubic centimeter (molecules $\cdot$ cm^{-3}). The ideal gas equation was used to obtain measurements of concentration by volume.

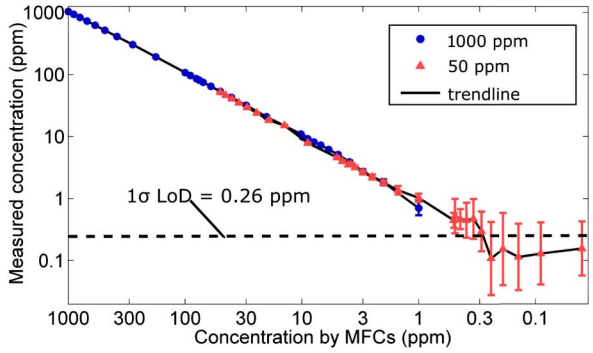

Fig. 8. Methane concentration measurements made using the 5 m long, 1000 μm bore diameter gas cell. These were calculated from the measured absorption data and known line strength and half-width values using Eqs. (3)–(5).

The frequency values ν can be calibrated using an etalon placed in the beam path; however, here the wavelength scale was obtained by taking the known peak wavelength values for the two-line maxima and interpolating the values in between. This procedure assumes that there is minimal pressure drop across the cell, such that the gas in the cell is all at room temperature.

The measured concentration values at each step, calculated from the measured absorption data using Eqs. (3) and (4), are shown in Fig. 8, plotted against concentration values calculated from the flow rates output by the MFCs. The different marker types correspond to measurements made using gas with base methane concentrations of 1000 ppm and 50 ppm. The standard deviation of 20 measurements made at each concentration step was used to determine the error bar of each data point. A limit of detection (LoD) was established by taking the mean of these standard deviation values and was found to be 0.26 ppm $\pm$ 0.12 ppm, as indicated by the black dashed line in Fig. 8.

A comparison was made between the Brewster aligned and normal, recessed windows. Each version was tested with a 5 m, 1000 μm bore diameter gas cell. The gas cell constructed using the Brewster aligned windows did not offer any performance advantage relative to those constructed using the recessed windows. This was primarily due to the fact that no interference fringes were observed in the detected signal. Additionally, because of the protrusion of window material over the edge of the fitting, the output end of a cell with Brewster aligned windows could not be positioned as closely to the detector as those with the recessed windows. This resulted in a relative reduction in the observed signal and a correspondingly worse NEA, as shown in Table 2.

The 1σ limit of detection for the 10 m cell constructed from the 1000 μm bore diameter waveguide was found to be 0.42 ppm $\pm$ 0.24 ppm. This is higher than was found for the 5 m long gas cell because, even though an increase in absorption was observed due to the increased path length, its NEA is much higher due to optical attenuation in the waveguide. The 1σ limit of detection for the 5 m path length cell constructed from the 300 μm bore diameter waveguide was found to be 0.76 ppm $\pm$ 0.42 ppm, which is higher again because of its higher NEA, without having the increase in sensitivity that the 10 m cell has. Even though the limit of detection is higher than either of the other two gas cells constructed with the 1000 μm bore diameter waveguide, the 300 μm bore diameter cell still works very well and offers a number of other

Table 2. Summary of Performance Parameters for the Three HSW Gas Cells

Cell Length (m)	Window[a]	Bore Diameter (μm)	Coil Diameter (cm)	NEA ×10^{-4}	LoD (ppm)
5	NR	1000	30	4.1	0.26
5	BA	1000	30	5.6	0.31
10	NR	1000	30	18	0.42
5	NR	300	15	17	0.76

[a]NR, normal recessed; BA, Brewster aligned.

significant advantages over the larger cells. In particular, it is much smaller and more flexible than the cells made from the 1000 μm bore diameter waveguide. This smaller footprint may be very important in terms of instrument design. HSWs with intermediate bore diameters are expected to offer performances in between the two extremes considered here. A summary of the performance parameters of the four cells is given in Table 2.

5. COMPARISON OF AN HSW GAS CELL WITH AN ASTIGMATIC HERRIOTT CELL

The performance of the 5 m long gas cell constructed from the 1000 μm bore diameter HSW was compared with that of an astigmatic Herriott cell with a folded optical path length of 30 m (146 passes) and a volume of ~400 ml. Light from the QCL was split with a BaF_2 beam splitter, which allowed both cells to be tested simultaneously using separate similar detectors. Typical pulses recorded with both cells containing 200 ppm methane are shown in Fig. 9 and clearly demonstrate the improved sensitivity of the 30 m path length Herriott cell. The spatial separation of the two traces on the x-axis (time) is due to the different arrival times of photons reaching the two detectors from the two cells.

The 1σ limit of detection of the Herriott cell was determined in the same manner as for the HSW cells discussed in Section 4.B and was found to be 35 ppb. Its NEA was calculated from the pulse data and was found to be 5.9×10^{-4}, which is slightly higher than the 4.1×10^{-4} NEA measured for the 5 m path length HSW gas cell made from the 1000 μm bore diameter waveguide. These values are similar to the value of 4×10^{-4} measured by Normand *et al.* [36], who used a similar spectrometer with a 10 m white cell.

A. Data Processing

To assess the long-term stability of the gas cells, pulse measurements were made over a period of 24 h at a data acquisition rate of 0.2 Hz. Figure 11(a) shows the mean pulse amplitude variation taken from the central 300 data points across each pulse recorded over this period for the two gas cells filled with air. The effect of averaging and long-term drift of the time series can be visualized using an Allan–Werle variance plot [44].

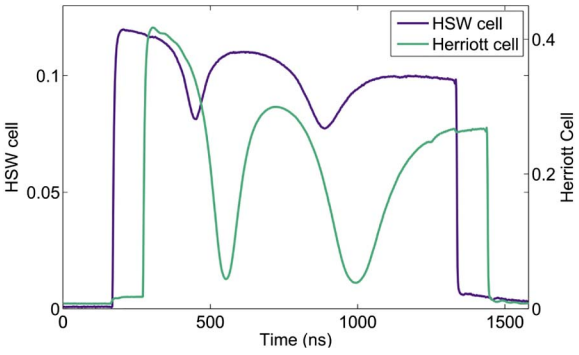

Fig. 9. Pulses in the presence of 200 ppm methane recorded simultaneously through an HSW cell and an astigmatic Herriott cell. The difference in arrival time of photons after passing through the two cells can be seen from the separation of the traces on the time (x) axis.

These plots typically show that an improvement in repeatability can be achieved with averaging up to some optimum level, after which the influence of drift takes over and repeatability diminishes with further averaging. Because of the typical distribution of the data, plots of the Allan–Werle deviation (square root of variance) are usually presented on log–log axes. The Allan–Werle deviations of the time-series data in Fig. 10(a) are shown in Fig. 10(b). The data show that averaging for a period of up to a few hundreds of seconds will improve repeatability but afterward drift dominates. The plateauing of the HSW data between averaging periods of ~200 s and 1000 s indicates that there is potential for further improvement of the limit of detection.

B. Response Time

The response time of both cells was assessed at a flow rate of 1000 sccm (1 l/min) using data recorded while 50 ppm methane filled and was evacuated from the cells. In order to improve the temporal resolution of the response time measurements, the data acquisition rate of the system was increased to 18 Hz (relative to the 0.5 Hz used in Section 4 and the 0.2 Hz used in Section 5.A). This was achieved by reducing the number of averages from 1000 to 100 and by reducing the pulse width to 300 ns, which was sufficient to capture one of the methane lines in the pair.

These reduced duration pulses require fewer data points per pulse and are therefore output at a significantly faster rate than the 800 ns pulses used in the previous sections. The data shown in Fig. 11 are the difference between maximum and minimum absorbance from each of the recorded pulses. The response time Δt is defined as the $t_{90} - t_{10}$ time, where t_{90} is the time at which the signal is at 90% of its maximum, and t_{10} is the time when the signal is at 10% of its maximum. Figure 11(a) shows the absorption data obtained through the HSW cell with a response time $\Delta t = 0.8$ s obtained for the rise and 0.7 s for the

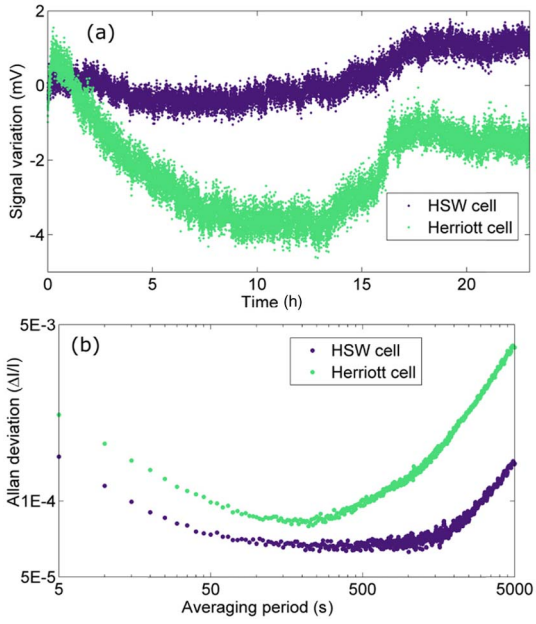

Fig. 10. (a) Mean pulse amplitude variation data for HSW and Herriott cells and (b) the Allan–Werle deviation of this data.

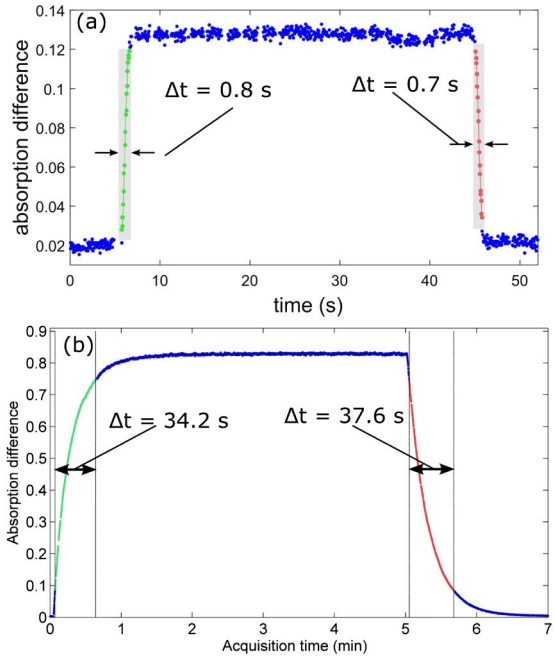

Fig. 11. Plots of the absorption difference recorded over time for (a) the HSW cell and (b) the Herriott cell as methane fills and is evacuated from the cells. The response time Δt is shown for both cells for both the rise and the fall.

fall. The measurement was repeated several times, and an average response time magnitude of $\Delta t = 0.8$ s was obtained for both the rise and the fall. Figure 11(b) shows the absorption data obtained through the Herriott cell with response times of $\Delta t = 34.2$ s and $\Delta t = 37.6$ s observed for the rise and the fall, respectively. The data here includes a delay in actuation of the MFCs. The Herriott cell data are less noisy than the HSW cell data due to its greater absorption sensitivity.

The response is more than an order of magnitude faster for the HSW cell compared to the Herriott cell due to its smaller internal volume, which was ~3.9 ml (for HSW only) compared with the Herriott cell's internal volume of ~400 ml. Another point also becomes apparent from this result: if the flow rate was much less than considered here, say 50 sccm, and the response time varies linearly with flow rate, then the response time of the HSW cell would be ~16 s and the response time of the Herriott cell would be ~700 s. According to the Allan–Werle deviation plot in Fig. 11(b), the performance of the HSW cell would still be very good, while the Herriott cell performance would be reduced due to the long averaging time being subject to the effects of drift. On the other hand, if the flow rate were increased, the response time of the Herriott cell would improve, whereas any improvement for the HSW cell would be limited due to its narrow bore. Its response at low flow rates, however, makes the HSW cell very useful for applications where there is naturally a low flow rate or low volume such as in medicine/healthcare.

6. DISCUSSION AND CONCLUSION

Hollow silica waveguides offer a potential solution to the demand for low-volume, fast-response-time gas cells, which also offer long interaction path lengths. Their construction makes them compatible with mid-infrared spectroscopy systems using QCLs or FTIR. Here we have presented three HSW gas cell configurations, which were each constructed using commercially available materials. A simple and elegant method of constructing gas and light entry and exit ports using customized commercially available gas fittings was demonstrated. These ports offer compatibility with other instrumentation and minimize the dead space at either end of the cell. The performance of the cells was assessed using a commercially available QCL spectroscopy system operating using the intrapulse down-chirp technique.

Limit of detection measurements were made using a network of mass flow controllers. The results showed that while increasing the waveguide length increases sensitivity, it does not necessarily improve the detection limit because of attenuation in the waveguide and the fact that this type of cell was detector noise limited. Therefore, there is an optimum waveguide length for a spectroscopic gas cell that also depends on the laser and detector that is used. The results showed that smaller bore waveguides can also be used for gas cell manufacture, albeit with a higher limit of detection. These are much more mechanically flexible and would be beneficial when developing compact instrumentation.

While the HSW gas cells lack the mechanical stability of the recently reported iHWGs [33], the problem was not an issue in this work because of the short time constant of the intrapulse measurement. Measurements are made across a pulse with durations of the order of hundreds of nanoseconds, whereas the effects of vibrations occur over much longer timescales (Hz–kHz). In addition, the path length and attenuation characteristics of these HSW gas cells are better than those yet reported for iHWGs. Attenuation within these HSW gas cells is still significant though, particularly with the smaller waveguides, and generally inferior to gas cells made of hollow-core PBGFs. However, the long response time of PBGF-based gas cells is currently prohibitive for most applications.

Another advantage provided by the short measurement time is the lack of speckle noise due to multimode interference that was experienced by, e.g., Chen *et al.* [24]. Although multimode transmission was observed, through speckle patterns measured at the output of the waveguide [35], this was not a significant issue. Since the spectroscopic acquisition is so fast, measurements are made across the laser pulses with durations of the order of hundreds of nanoseconds, no speckle noise associated with intermode interference was observed in the time domain and measurements were instead limited by detector noise.

The HSW gas cells that we have developed offer fast response times, with a response time of 0.8 s measured for a flow rate of 1000 sccm with a 5 m long cell with a 1000 μm bore diameter. The best case NEA and limit of detection was observed also with the 5 m long, 1000 μm bore diameter HSW cell. Its NEA was measured to be 4.1×10^{-4} and its 1σ LoD was measured to be 0.26 ppm for an averaging period of 2 s. Allan–Werle analysis indicates that this NEA value can be improved to $\sim 7 \times 10^{-5}$ for an optimum averaging period of 300–600 s.

For research data or other materials referred to in this paper, please access the Cranfield Online Research Data repository at doi: 10.17862/cranfield.rd.3492908.

Funding. Technology Strategy Board (TSB) (100846); Engineering and Physical Sciences Research Council (EPSRC) (EP/H02252X).

REFERENCES

1. H. I. Schiff, G. I. Mackay, and J. Bechara, "The use of tunable diode laser absorption spectroscopy for atmospheric measurements," in *Air Monitoring by Spectroscopic Techniques*, M. W. Sigrist, ed. (Wiley, 1994).
2. D. Masiyano, J. Hodgkinson, and R. P. Tatam, "Use of diffuse reflections in tunable diode laser absorption spectroscopy: implications of laser speckle for gas absorption measurements," Appl. Phys. B **90**, 279–288 (2008).
3. J. Hodgkinson and R. P. Tatam, "Optical gas sensing: a review," Meas. Sci. Technol. **24**, 1–59 (2013).
4. J. Faist, F. Capasso, D. L. Sivco, C. Sirtori, A. L. Hutchinson, and A. Y. Cho, "Quantum cascade laser," Science **264**, 553–556 (1994).
5. F. Capasso, "High-performance midinfrared quantum cascade lasers," Opt. Eng. **49**, 111102 (2010).
6. J. B. McManus, M. S. Zahniser, D. D. Nelson, Jr., J. H. Shorter, S. Herndon, E. Wood, and R. Wehr, "Application of quantum cascade lasers to high-precision atmospheric trace gas measurements," Opt. Eng. **49**, 111124 (2010).
7. L. Wang and B. Mizaikoff, "Application of multivariate data-analysis techniques to biomedical diagnostics based on mid-infrared spectroscopy," Anal. Bioanal. Chem. **391**, 1641–1654 (2008).
8. M. R. McCurdy, Y. Bakhirkin, G. Wysocki, R. Lewicki, and F. K. Tittel, "Recent advances of laser-spectroscopy-based techniques for applications in breath analysis," J. Breath Res. **1**, 014001 (2007).
9. E. L. Normand, R. J. Stokes, K. Hay, B. Foulger, and C. Lewis, "Advances in quantum cascade lasers for security and crime fighting," Proc. SPIE **7838**, 78380A (2011).
10. R. H. Micheels, K. Richardson, D. J. Haan, and J. A. Harrington, "FTIR based instrument employing a coiled hollow waveguide cell for rapid field analysis of volatile organic compounds," Proc. SPIE **3540**, 66–74 (1999).
11. B. Cummings, M. L. Hamilton, L. Ciaffoni, T. R. Pragnell, R. Peverall, G. A. D. Ritchie, G. Hancock, and P. A. Robbins, "Laser-based absorption spectroscopy as a technique for rapid in-line analysis of respired gas concentrations of O_2 and CO_2," J. Appl. Physiol. **111**, 303–307 (2011).
12. C. M. Charlton, B. T. Thompson, and B. Mizaikoff, "Hollow waveguide infrared spectroscopy and sensing," in *Frontiers in Chemical Sensors: Novel Principles and Techniques*, G. Orellana and M. C. Moreno-Bondi, eds. (Springer-Verlag, 2005).
13. J. A. Harrington, "A review of IR transmitting hollow waveguides," Fiber Integr. Opt. **19**, 211–227 (2000).
14. Y. Matsuura, T. Abel, J. Hirsch, and J. A. Harrington, "Single-bore hollow waveguide for delivery of near single mode IR laser radiation," Electron. Lett. **30**, 1688–1690 (1994).
15. R. George and J. A. Harrington, "Infrared transmissive, hollow plastic waveguides with inner Ag/AgI coatings," Appl. Opt. **44**, 6449–6455 (2005).
16. Y. Matsuura, T. Abel, and J. A. Harrington, "Optical properties of small-bore hollow glass waveguides," Appl. Opt. **34**, 6842–6847 (1995).
17. J. A. Harrington, "Theoretical foundations of infrared fiber optic transmission: hollow-core fibers," in *Infrared Fiber Optics and Their Applications* (SPIE, 2004).
18. C. M. Bledt, J. A. Harrington, and J. M. Kriesel, "Multilayer silver/dielectric thin-film coated hollow waveguides for sensor and laser power delivery applications," Proc. SPIE **8218**, 82180H (2012).
19. Polymicro Technologies, Phoenix, Arizona, USA, accessed 11 May, 2016, http://www.molex.com/molex/products/group?channel=products&key=polymicro.
20. G. J. Fetzer, A. S. Pittner, W. L. Ryder, and D. A. Brown, "Tunable diode laser absorption spectroscopy in coiled hollow optical waveguides," Appl. Opt. **41**, 3613–3621 (2002).
21. C. Charlton, F. de Melas, A. Inberg, N. Croitoru, and B. Mizaikoff, "Hollow-waveguide gas sensing with room-temperature quantum cascade lasers," IEE Proc. **150**, 306–309 (2003).
22. C. Young, S.-S. Kim, Y. Luzinova, M. Weida, D. Arnone, E. Takeuchi, T. Day, and B. Mizaikoff, "External cavity widely tunable quantum cascade laser based hollow waveguide gas sensors for multianalyte detection," Sens. Actuators B **140**, 24–28 (2009).
23. B. T. Thompson, A. Inberg, N. Croitoru, and B. Mizaikoff, "Characterization of a mid-infrared hollow waveguide gas cell for the analysis of carbon monoxide and nitric oxide," Appl. Spectrosc. **60**, 266–271 (2006).
24. J. Chen, A. Hangauer, R. Strzoda, and M. C. Amann, "Resolution limits of laser spectroscopic absorption measurements with hollow glass waveguides," Appl. Opt. **49**, 5254–5261 (2010).
25. F. Poletti, M. N. Petrovich, and D. J. Richardson, "Hollow-core photonic bandgap fibres: technology and applications," Nanophotonics **2**, 315–340 (2013).
26. F. Benabid, F. Couny, J. C. Knight, T. A. Birks, and P. St.J. Russell, "Compact, stable and efficient all-fibre gas cells using hollow-core photonic crystal fibres," Nature **434**, 488–491 (2005).
27. J. P. Parry, B. C. Griffiths, N. Gayraud, E. D. McNaghten, A. M. Parkes, W. N. MacPherson, and D. P. Hand, "Towards practical gas sensing with micro-structured fibres," Meas. Sci. Technol. **20**, 075301 (2009).
28. J. A. Nwaboh, J. Hald, J. K. Lyngsø, J. C. Petersen, and O. Werhahn, "Measurements of CO_2 in a multipass cell and in a hollow-core photonic bandgap fiber at 2 μm," Appl. Phys. B **110**, 187–194 (2013).
29. N. V. Wheeler, A. M. Heidt, N. K. Baddela, E. Numkam Fokoua, J. R. Hayes, S. R. Sandoghchi, F. Poletti, M. N. Petrovich, and D. R. Richardson, "Low loss and low bend sensitivity mid-IR guidance in a hollow core-photonic bandgap fiber," Opt. Lett. **39**, 295–298 (2014).
30. OmniGuide, Inc., accessed 11 May, 2016, http://www.omni-guide.com/.
31. Y. Fink, J. N. Winn, S. Fan, C. Chen, J. Michel, J. D. Joannopoulos, and E. L. Thomas, "A dielectric omnidirectional reflector," Science **282**, 1679–1682 (1998).
32. C. Charlton, B. Temelkuran, G. Dellemann, and B. Mizaikoff, "Midinfrared sensors meet nanotechnology: trace gas sensing with quantum cascade lasers inside photonic band-gap hollow waveguides," Appl. Phys. Lett. **86**, 194102 (2005).
33. A. Wilk, J. C. Carter, M. Chrisp, A. M. Manuel, P. Mirkarimi, J. B. Alameda, and B. Mizaikoff, "Substrate-integrated hollow waveguides: a new level of integration in mid-infrared gas sensing," Anal. Chem. **85**, 11205–11210 (2013).
34. P. R. Fortes, A. Wilk, F. Seichter, M. Cajlakovic, S. Koestler, V. Ribitsch, U. Wachter, J. Vogt, P. Radermacher, C. Carter, I. M. Raimundo, Jr., and B. Mizaikoff, "Combined sensing platform for advance diagnostics in exhaled mouse breath," Proc. SPIE **8570**, 85700Q (2013).
35. D. Francis, J. Hodgkinson, B. Livingstone, and R. P. Tatam, "Quantum cascade laser light propagation through hollow silica waveguides," Appl. Phys. B **119**, 75–86 (2015).
36. E. Normand, M. McCullogh, G. Duxbury, and N. Langford, "Fast, real-time spectrometer based on a pulsed quantum cascade laser," Opt. Lett. **28**, 16–18 (2003).
37. M. Saito and T. Kato, "Fast infrared spectrometer for flowing gases by the use of a hollow fiber and a PtSi sensor array," Infrared Phys. Technol. **48**, 53–58 (2006).
38. D. Francis, J. Hodgkinson, and R. P. Tatam, "Hollow fibre waveguide gas cells," U.S. patent PCT/GB2016/050789 (22 March 2016).
39. Cascade Technologies, accessed 11 May 2016, http://www3.emersonprocess.com/cascade-technologies.
40. J. Manne, W. Jäger, and J. Tulip, "Sensitive detection of ammonia and ethylene with a pulsed quantum cascade laser using intra and inter-pulse spectroscopic techniques," Appl. Phys. B. **94**, 337–344 (2009).
41. M. T. McCulloch, E. L. Normand, N. Langford, G. Duxbury, and D. A. Newnham, "Highly sensitive detection of trace gases using the time-resolved frequency downchirp from pulsed quantum-cascade lasers," J. Opt. Soc. Am. B **20**, 1761–1768 (2003).
42. Accessed 11 May, 2016, www.swagelok.com.
43. L. S. Rothman, R. R. Gamache, A. Goldman, L. R. Brown, R. A. Toth, H. M. Pickett, R. L. Poynter, J. M. Flaud, C. Camy-Peyret, A. Barbe, N. Husson, C. P. Rinsland, and M. A. H. Smith, "The HITRAN database: 1986 edition," Appl. Opt. **26**, 4058–4097 (1987).
44. P. Werle, R. Mücke, and F. Slemr, "The limits of signal averaging in atmospheric trace-gas monitoring by tunable diode-laser absorption spectroscopy (TDLAS)," Appl. Phys. B **57**, 131–139 (1993).